Deep-sea stylasterid $\delta^{18}O$ and $\delta^{13}C$ maps inform sampling scheme for paleotemperature reconstructions

Theresa M. King[1], Brad E. Rosenheim[1], and Noel P. James[2]

[1]College of Marine Science, University of South Florida, St. Petersburg, 33701, USA
[2]Department of Geological Sciences and Geological Engineering, Queens University, Kingston, K7L 3N6, Canada

Correspondence to: Theresa M. King (theresaking@usf.edu)

Abstract. Deep-sea corals have the potential to provide high-resolution paleotemperature records to evaluate oceanographic changes in settings that are vulnerable to current and future ocean warming. The isotopic records preserved in coral skeletal carbonate, however, are limited by their large offsets from isotopic equilibrium with seawater. These "vital effects" are the result of biological influences (kinetic and metabolic) on the calcification of coral skeletons and are well known to drive oxygen and carbon stable isotope ratios ($\delta^{18}O$ and $\delta^{13}C$, respectively) away from an isotopic signature in equilibrium with environmental variables. Additionally, vital effects of deep-sea branching corals are not well understood, thus hindering the utility of paleoceanographic archives with a vast latitudinal range. This contribution describes the likely growth structure of a deep-sea stylasterid coral taxon and demonstrates the optimal sampling location for its use in paleotemperature reconstructions. We sampled two coral specimens via cross sections through their primary growth axes to create skeletal $\delta^{18}O$ and $\delta^{13}C$ maps. Such maps reveal a consistent trend of increasing isotopic values toward the innermost portion of the coral slices; the average center values being ~1‰ closer to seawater equilibrium values than a traditional bulk sample. The difference between the higher center and lower bulk $\delta^{18}O$ values result in a temperature difference as much as 5.1° C (±1.8° C) between the sampling methods. These results support a two-step biomineralization consisting of a rapid initial skeletal construction (stronger vital effects), followed by a slower infilling concentrated towards the center (weaker vital effects) not yet described for this coral taxon. We anticipate this work will initiate efforts to sample deep-sea branching corals and potentially inform advanced visualization techniques (e.g., computed tomography scans) to achieve the most accurate paleotemperature reconstructions possible.

1 Introduction

Robust paleoceanographic temperature proxies are fundamental to understanding past climate changes and sensitivities. Foundational work developed the theory and application of the oxygen isotope paleothermometer, which was applied to marine biogenic carbonates including foraminiferal tests and shallow water corals (Urey, 1947; McCrea, 1950; Epstein et al., 1953; Emiliani, 1955; Shackleton, 1967; Emiliani et al., 1978). All archives have limits in geographic distribution despite their ability

to lengthen the time domain of our paleoceanographic records. On the Antarctic margin, for instance, foraminifera are not widely present in marine sediment cores. Scleractinian zooxanthellate corals are limited to lower latitudes. Deep-sea azooxanthellate corals have been used to elucidate ocean history on different time scales (Adkins et al., 1998; Robinson et al., 2005; Robinson and van de Flierdt, 2009; Burke and Robinson, 2012; Chen et al., 2020), but normally the extraction of continuous records from individual colonies has been precluded by the complexity of growth habit and the fidelity of elemental and isotopic records archived in their skeletons (Weber, 1973; Wisshak et al., 2009; Robinson et al., 2014). Corals can incorporate high resolution geochemical records over decades to millennia while remaining fixed to the seafloor; this is especially useful to observe regional and global processes causing ocean water masses to heave and shoal at timescales over which the coral is alive (Andrews et al., 2002; Druffel et al., 1990; Druffel, 1997; Griffin and Druffel, 1989; Risk et al., 2002). Such archives are crucial for paleotemperature reconstructions.

Biomineralization of carbonate skeletons records both environmental information (which we treat herein as "signal") and biological effects (noise, also known as "vital effects"), the latter of which must be understood to obtain high-fideltiy records of ocean change. Vital effects can obscure environmental information stored in skeletal records as oxygen and carbon stable isotope ratios ($\delta^{18}O$ and $\delta^{13}C$, respectively). Slow rates of calcification allow for carbon and oxygen isotopes of solid carbonate to approach isotopic equilibrium between skeleton and seawater, a state governed by thermodynamics (McConnaughey, 1989a). Biological calcification, however, includes nonequilibrium fractionation which cannot be interpreted directly as environmental signal (Weber and Woodhead, 1970). Early research on corals demonstrated that isotopic variability can be caused by metabolic fractionation, kinetic fractionation, or a combination of both (McConnaughey, 1989a). The metabolic fractionation is characterized by a change in carbon isotope composition of the dissolved inorganic carbon pool from which the coral calcifies via incorporation of the products of respiration and photosynthesis of algal symbionts or respiration of the coral itself (Swart, 1983; McConnaughey, 1989a). The kinetic fractionation is described as a product of the kinetic isotope effect: discrimination against heavy oxygen and carbon isotopes during hydration and hydroxylation of CO_2 during biomineralization (McConnaughey, 1989b). Rapid calcification results in greater disequilibrium of skeletal $\delta^{18}O$ and $\delta^{13}C$ as the CO_2 does not have sufficient time to equilibrate with ambient seawater before being incorporated into the skeleton (McConnaughey, 1989b). Additional mechanisms for vital effects have been identified more recently, including a biologically mediated pH gradient across coral cell walls (Adkins et al., 2003). Rapid biomineralization drives the pH of internal calcifying fluid toward higher values, increasing the pumping of CO_2, and consequently maximizing fractionation of carbon isotopes (Adkins et al., 2003). Chen et al. (2018) then combined these findings with an additional constraint of kinetic fractionation by the carbonic anhydrase enzyme which catalyzes the hydration and hydroxylation of CO_2 and constructed the most comprehensive model for biomineralization to date.

Because coral specimens from varied ocean depths and latitudes have a strong linear relationship between skeletal $\delta^{18}O$ and $\delta^{13}C$ values (Smith et al., 2000; Emiliani et al., 1978; Heikoop et al., 2000; Mikkelsen et al., 2008; McConnaughey, 1989a),

vital effects have been employed to discern trends in $\delta^{18}O$ and $\delta^{13}C$ records from deep-sea corals. Isotopic records have largely demonstrated sensitivity to variable rates of calcification. Early work by (Emiliani et al., 1978) examined the $\delta^{18}O$ and $\delta^{13}C$ recorded by a solitary scleractinian coral and found that both isotopic ratios trended toward higher values from bottom to top of the coral and interpreted this as a slowing growth rate with time, approaching isotopic equilibrium. Additional work on solitary scleractinians by Adkins et al. (2003) employed a microsampling approach for $\delta^{18}O$ and $\delta^{13}C$ that determined the lowest isotopic values occurred at trabecular centers which exhibited the most rapid rates of calcification and were farthest from equilibrium. Bamboo corals sampled across and along their vertical growth axes exhibited low $\delta^{18}O$ and $\delta^{13}C$ values near the innermost portion of the coral and at the distal tips (Hill et al., 2011). Faster calcification in these regions, however, were not supported by calculated growth rates, and there was no consistency among regions of maximum growth rates for a single specimen (Hill et al., 2011). A study by Wisshak et al. (2009) and another by Samperiz et al. (2020) sampled stylasterid corals in transects similar to Hill et al. (2011) and resulted in $\delta^{18}O$ and $\delta^{13}C$ trends with lowest values in the innermost portion of the main coral trunk and at the distal growth tips, supporting rapid growth in those regions. However, Samperiz et al. (2020) noted variability among the $\delta^{18}O$ and $\delta^{13}C$ values within a single growth band (which should represent contemporaneous calcification) as well as variability in isotopic fractionation among different genera and species of stylasterid, supporting heterogeneous calcification. Cumulatively, these results obscure best practices for colony-scale sampling of deep-sea corals for isolating vital effects to develop robust temperature reconstructions.

Here we focus on the small-scale isotopic changes in a stylasterid taxon with the aim of understanding the best sampling approach for accurate paleotemperature reconstructions using a single species. Stylasterids are ubiquitous in both latitudinal and depth range, yet remain underrepresented in paleoceanographic reconstructions, due in part to the lack of understanding of calcification processes (Cairns, 1992). Studies have recently begun to demonstrate the utility of deep-sea stylasterid taxa as reliable archives of ocean temperature via $\delta^{18}O$ and trace metals (Samperiz et al., 2020 and Stewart et al., 2020, respectively) as well as productivity/seawater nutrient content via skeletal Ba/Ca (Kershaw et al., 2023). To apply such archives to high-resolution reconstructions, however, a thorough understanding of the small-scale variability in vital effects is paramount. Here we establish a link between deep-sea coral growth and isotopic changes, using two deep-dwelling (400 to 600 m) stylasterid coral specimens, *Errina fissurata*, to create $\delta^{18}O$ and $\delta^{13}C$ maps over surfaces perpendicular to and along vertical growth axes. We complement recent work by Samperiz et al. (2020) that has demonstrated the utility of stylasterids to accurately record changes in ocean temperatures by isolating kinetic effects in deep, azooxanthellate stylasterids. We compare our skeletal maps to isotopic trends modelled from hypothesized coral growth scenarios and determine that although contradictory to previous research, the isotopic values most representative of environmental signals are recorded in the innermost portion of the coral stems. Ultimately, we prescribe targeted sampling, avoiding the use of bulk drilling methods for the most accurate paleotemperature reconstructions for *E. fissurata*.

2 Methods

2.1 Study location and specimen collection

The Ross Sea is a region of bottom water formation for the worlds' oceans, a characteristic that influences the local oceanography in which the stylasterids live. The region experiences seasonal katabatic winds that create sea ice-forming polynyas, which in turn, create High Salinity Shelf Water through the process of brine rejection (Kurtz and Bromwich, 1985; Picco et al., 2000). The High Salinity Shelf Water flows along the western Ross Sea and out to the shelf edge where it mixes with upwelled modified Circumpolar Deep Water, resulting in a component of dense Antarctic Bottom Water that spills down the continental slope (Gordon et al., 2009; Jacobs et al., 1970; Sandrini et al., 2007).

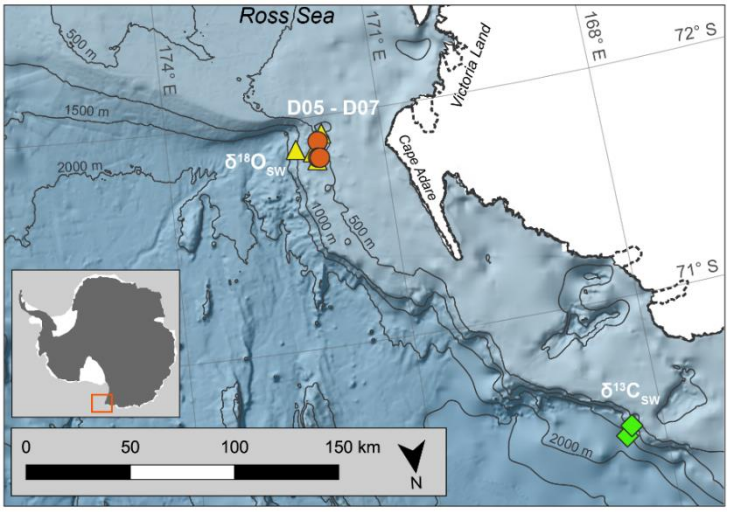

Figure 1: Map of coral collection sites. D05–D07 represent dredge sites during NBP07-01 from which coral samples were collected on the outer western Ross Sea continental shelf. The diamonds and triangles mark the stations used to calculate the seawater isotopic ratios ($\delta^{13}C_{sw}$ and $\delta^{18}O_{sw}$; Table S2 in the Supplement). Antarctic landmass and ice sheets are colored white (Gerrish et al., 2022) with the coastline marked by a solid black line, and ice sheet grounding line denoted by a dotted black line (Mouginot et al., 2017). Bathymetric contours are in increments of 500 m (Arndt et al., 2013). Antarctic inset denotes sampling site marked by red box. Map was created using the Quantarctica data set collection within QGIS (Matsuoka et al., 2021).

The stylasterid coral specimens for this study were collected aboard the U.S. Antarctic Program expedition NBP07-01 near Cape Adare in the western Ross Sea. Seamounts on the outer continental shelf were dredged at a water depth ranging 400 m to 600 m and the corals used here were from the fifth through seventh dredges (D05–D07; Fig. 1, Table 1). The recovered stylasterid corals were predominantly *Errina* spp., most likely *Errina fissurata* based on morphological descriptions (Cairns, 1983a, b, 1991) and scanning electron microscopy (SEM). Specimens were recovered both alive and dead (as evidenced by their pigmentation), some with growth tips intact. For this study, one live-collected and one dead-collected stylasterid were selected (EA-11 and EA-12, respectively), targeting the longest whole specimens ranging from ~9 to 10 cm long (Fig. 2).

2.2 Coral sampling and isotope analysis

The stylasterid specimens were sampled for stable oxygen and carbon isotope measurements ($\delta^{18}O$ and $\delta^{13}C$, respectively) over cross sections of their major growth axes. A Gryphon diamond band saw was used to slice discs measuring approximately 2–3 mm thick from each specimen's main stems (three from EA-11 and two from EA-12; Fig. 2). Additionally, a longer 8 mm

thick section was cut from the lower main stem of EA-11 (EA-11d; Fig. 2). This disc was sliced in half lengthwise with the band saw and sampled along the vertical face. Each coral disc was sonicated in DI water until no remaining loose particles were released then dried in a 50° C oven for 24 hours. The coral discs were then drilled over their surfaces with a New Wave MicroMill system at grid spacing that varied between 1 and 1.5 mm, based on the diameter of the slice and ampullae in the disc. The MicroMill was configured with a 0.5 mm round carbide bur bit for each hole that plunged to a maximum depth of 1 mm, just far enough to obtain enough carbonate material for analysis (~80–120 µg $CaCO_3$). The carbonate powder from each hole was transferred to vials and the sample hole and stylasterid surface were cleaned with compressed air or nitrogen to remove any residual powder between drilling intervals.

Latitude (°S)	Longitude (°E)	Water Depth (m)	Dredge	Temperature (°C)	$\delta^{18}O$ seawater (‰, SMOW)	$\delta^{13}C$ seawater (‰, PDB)
71.89	171.9	490-593	D05	-0.10 ± 0.09	-0.26 ± 0.06	0.66 ± 0.05
71.82	171.92	518-643	D06			
71.82	171.9	489-599	D07			

Table 1: Sample collection data including approximate coordinates of dredges, the range of water depths sampled, names of each dredge, and approximate seawater properties. Temperature is averaged for dredge depth range using measurements from nearby AnSlope stations (Visbeck, 2015; Jacobs, 2015; Gordon, 2016). The corresponding potential temperatures and salinities for this depth range were used to determine the $\delta^{18}O$ of the seawater based on values reported by Jacobs et al. (1985) for Antarctic margin water masses. The seawater $\delta^{13}C$ is an average of values reported for the same depth range from nearby World Ocean Circulation Experiment stations (WOCE, 2002; Fig. S1 in the Supplement).

Figure 2: Whole coral specimens EA-11 (left) and EA-12 (right). EA-11 was live-collected, and EA-12 was dead. Sample discs are labelled, and the corresponding isotope maps are in Fig. 3.

The sample vials were flushed with helium and acidified with phosphoric acid at 50° C to generate CO_2 that was analyzed at the University of South Florida College of Marine Science using a Thermo Scientific MAT 253 stable isotope ratio mass spectrometer with a Gas Bench II preparatory device. All reported values are in standard delta (δ) notation and reported as per mil (‰). Laboratory reference materials Borba ($\delta^{13}C$: 2.89 ‰, $\delta^{18}O$: -6.15 ‰), TSF-1 ($\delta^{13}C$: 1.95 ‰, $\delta^{18}O$: -2.20 ‰), and Leco ($\delta^{13}C$: -15.44 ‰, $\delta^{18}O$: -20.68 ‰), were used for instrument correction and normalizing to the Pee Dee Belemnite scale (PDB), and an internal Antarctic coral standard was used for quality control. The analytical uncertainty (1σ) of the MAT 253 during this study was ±0.083 ‰ $\delta^{13}C$ and ±0.064 ‰ $\delta^{18}O$.

2.3 Mineralogical analysis

Two separate *E. fissurata* specimens were sampled for mineralogical analysis via X-ray diffraction (XRD), one live-collected and one dead-collected. Two samples were collected from each specimen, one in the center, white region and the other in the mid to outer pink region. The samples were ground, mixed with a quartz standard, and smeared on a glass slide. They were analyzed on a Malvern Panalytical Empyrean Multipurpose Diffractometer at Queen's University Facility for Isotope Research, Ontario, Canada. Original total mineralogy was ascertained by running from 20.0–45.0 2θ. Detailed mineralogy was determined by running from 34.0–35.5 2θ. The reported relative mineralogical amounts are semi-quantitative.

3 Results

The interior coral skeletons lacked any visible banded growth structure that we expected to see in the manner of Samperiz et al. (2020) and Wisshak et al. (2009). Instead, the corals were characterized by a central white section, surrounded by shades of pink in the mid to outer sections (Figs. 2 and 3). The replacement of a high-density growth banding structure with the observed color blocking is an obstacle to estimating the amount of time over which these corals have been growing. Thus, researchers aiming to employ this coral taxon must employ additional radiometric dating techniques (e.g., Cheng et al., 2000) that are beyond the scope of this work. Although there were no visible banding targets for sampling stable isotopes, the grid spacing of our sampling scheme allowed for microdrilling of several representative samples of both pink and white areas across each coral slice (Fig. S1 in the Supplement).

	$\delta^{18}O$ (‰, PDB)		$\delta^{13}C$ (‰, PDB)		
Coral Slice	Maximum	Minimum	Maximum	Minimum	n
EA-11a	2.48	0.65	-3.72	-9.56	17
EA-11b	2.18	0.87	-4.34	-8.61	24
EA-11c	2.64	1.08	-2.84	-8.54	20
EA-11d*	2.87	0.66	-2.64	-8.68	37
EA-12a	2.81	0.60	-3.19	-8.18	17
EA-12b	2.53	0.82	-3.00	-8.02	25
All	2.87	0.60	-2.64	-9.56	140
Linear Regression (All data)	Slope	Intercept	R^2	p-value	n
	2.88 (± 0.14)	-10.94 (± 0.22)	0.76	< 0.001	140

Table 2: Summary data for *E. fissurata* and regression statistics for the resulting compilation. The * signifies EA-11d as the slice that was cut parallel to the growth axis, unlike the rest of the slices that were sampled perpendicularly.

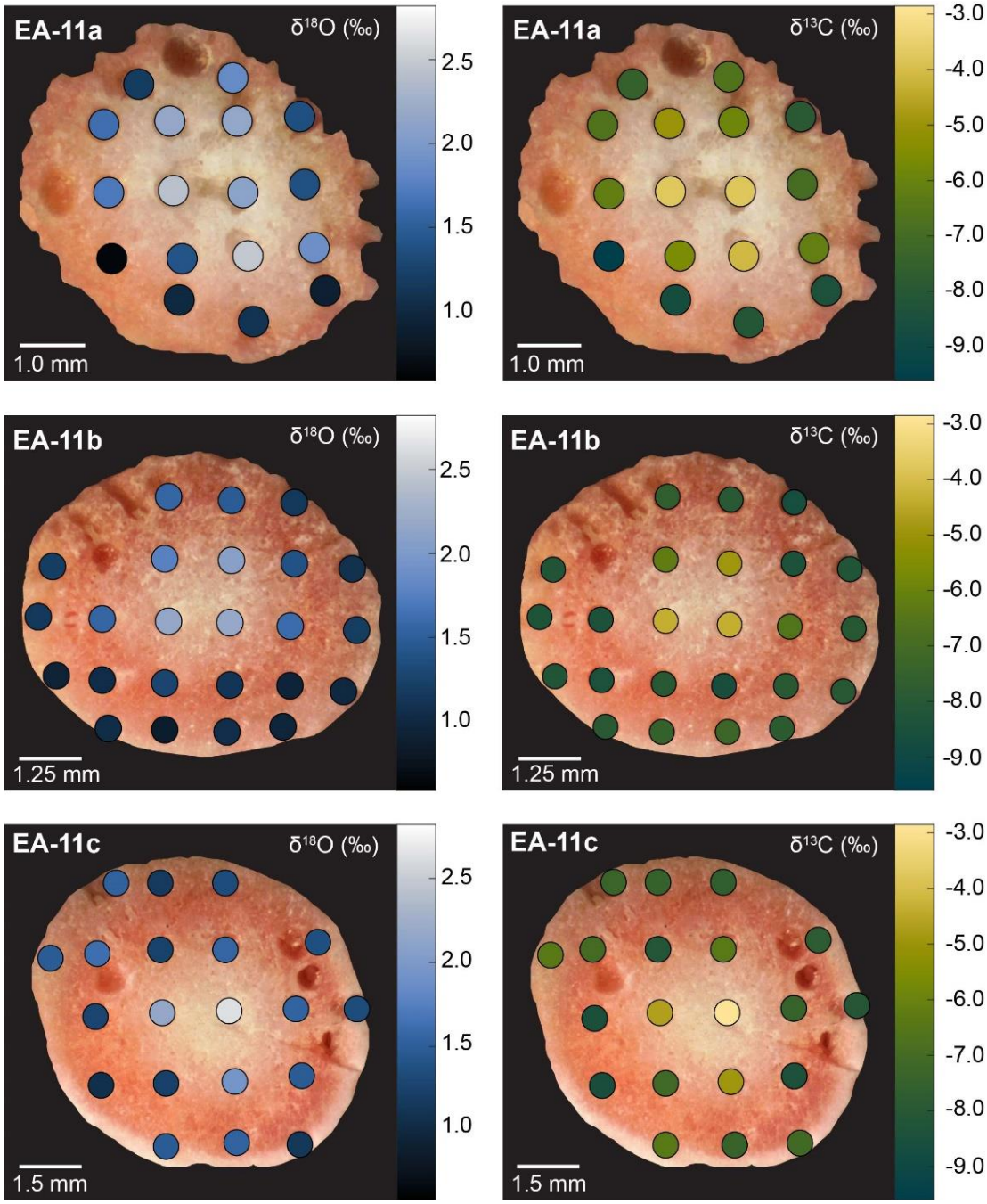

Figure 3: Stable isotope ratio maps for slices from specimens EA-11 and EA-12. Each horizontal pair of images show data from the same coral slice: the left column depicts $\delta^{18}O$ values and the right column $\delta^{13}C$ values. The measurements are presented as colored circles on each slice with corresponding adjacent color bar. Values are expressed in per mil (‰) relative to PDB, and analytical uncertainty (1σ) during this study was ±0.064 ‰ $\delta^{18}O$ and ±0.083 ‰ $\delta^{13}C$. All slices exhibit the same feature of the highest isotopic values toward the inner white section, which is not always the geometric center of the slice.

3.1 Stable carbon and oxygen isotope trends

Each coral slice exhibits a wide range of stable carbon and oxygen isotope ratios that are higher in the center, white section, and lower in the outer pink section of the coral (Fig. 3). For specimen EA-11, the ranges in $\delta^{18}O$ and $\delta^{13}C$ values across slices EA-11a through EA-11c are ~1.5 ‰ and ~5.2 ‰, respectively. This variability is too large to produce accurate paleoceanographic records without knowledge of where the most accurate, or closest

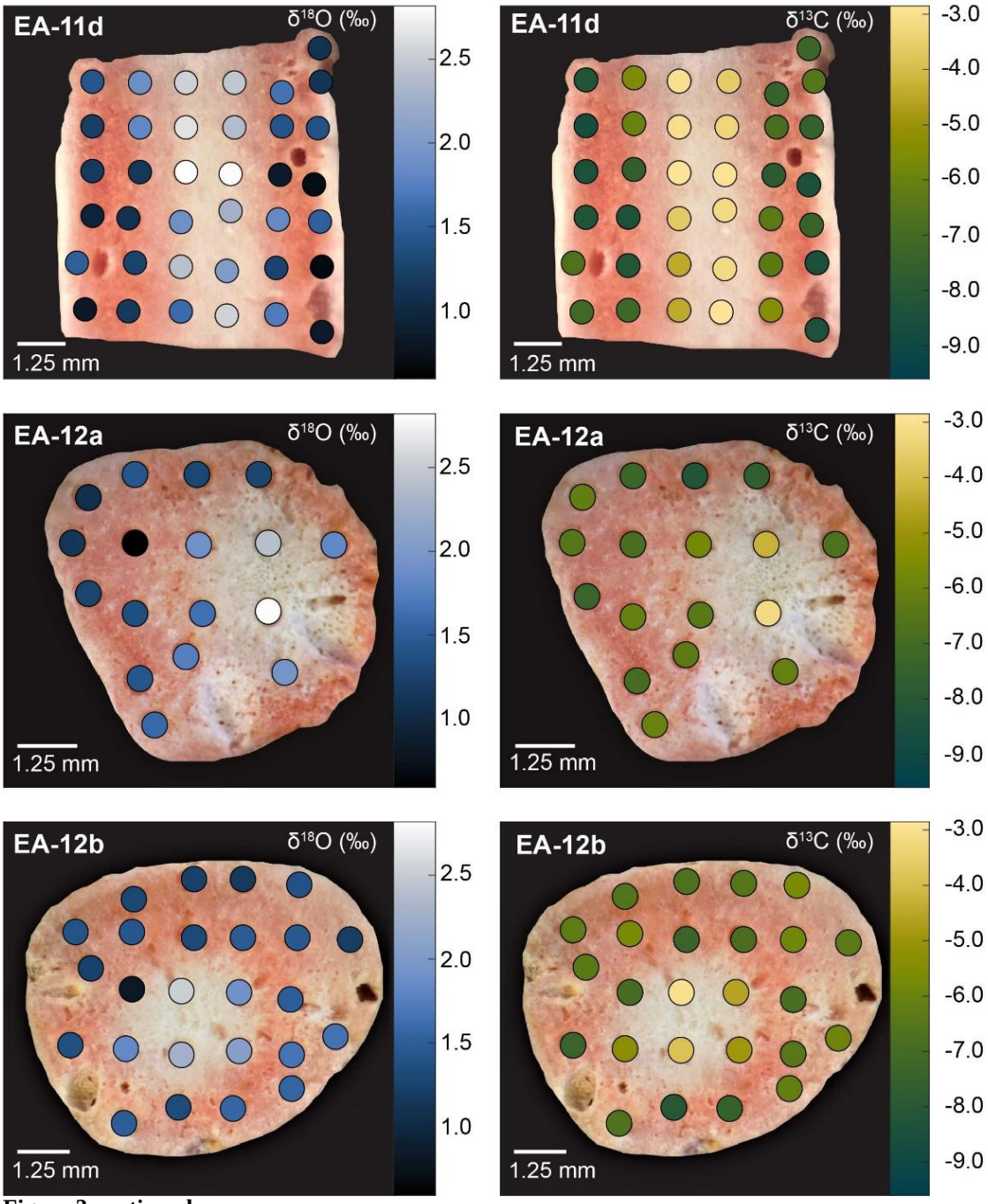

Figure 3 continued.

to that of an environmental signal, is preserved in the coral skeleton. The slightly larger range of $\delta^{18}O$ and $\delta^{13}C$ values observed over EA-11d (2.2 ‰ and 6.0 ‰, respectively) is not as surprising as it could be due to the sampling scheme for this slice covering a larger vertical distance of coral than the others (i.e., transecting more time intervals). The compilation of EA-11 $\delta^{18}O$ values ranges

from 0.65 ‰ to 2.87 ‰, and the $\delta^{13}C$ values range from -9.56 ‰ to -2.64 ‰, with the minimum values exhibited by EA-11a (nearest the tip) and maximum values by EA-11d (far from the tip; Table 2). Although this trend is not surprising (see Samperiz et al., 2020), if we consider "bulk" values that would be obtained by more traditional coral drilling methods, which average isotopic compositions by drilling into the side of a coral, there is no significant change in either isotopic composition up-coral (Fig. 4).

For specimen EA-12, the range of $\delta^{18}O$ and $\delta^{13}C$ values over each of the slices is on the order of ~2 ‰ and ~5 ‰, similar to EA-11 (Table 2). The entire range of measured EA-12 $\delta^{18}O$ values is 0.60‰ to 2.81‰, and $\delta^{13}C$ values range from -8.18 ‰ to -3.00 ‰. Minimum $\delta^{18}O$ and $\delta^{13}C$ values for EA-12 were both exhibited by slice EA-12a, nearest the tip. The maximum values, however, were not on the same slice (maximum $\delta^{18}O$ at EA-12a and maximum $\delta^{13}C$ at EA-12b). Similar to EA-11, EA-12 also exhibits variability within each slice; however, this also leads to the bulk calculations not being significantly different from each other up-coral (Fig. 4). Looking closer at the individual slices from each coral, the variable stable isotope compositions are significant, i.e., the minimum and maximum values measured on each slice are well beyond the analytical uncertainty (Figs. 4 and 5). This supports that all measurements consistently demonstrate significantly higher $\delta^{18}O$ and $\delta^{13}C$ values in the center of each slice (Figs. 3 and 5).

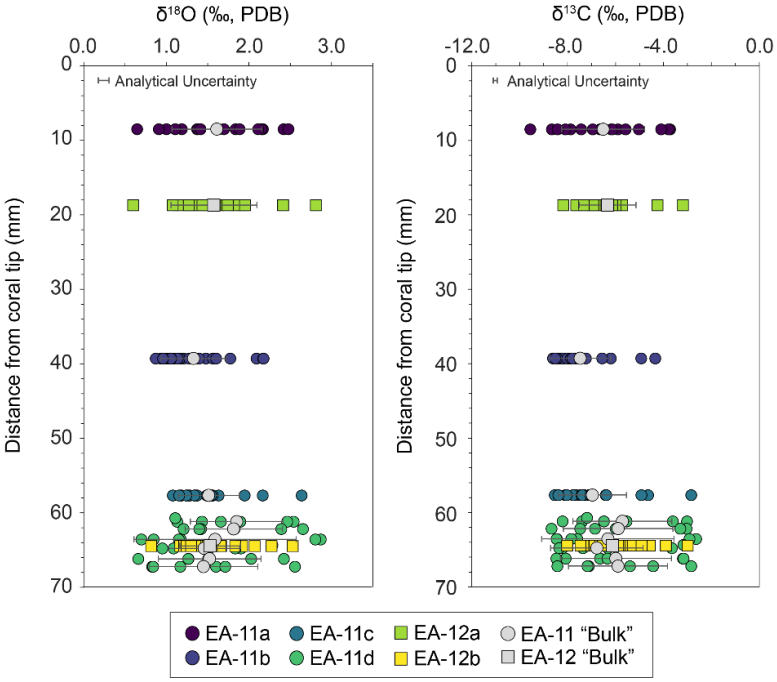

Figure 4: Stable isotope ratios from each slice ($\delta^{18}O$ on left and $\delta^{13}C$ on right) versus distance from the coral tips. A "bulk" value was calculated as the average for each slice (except for EA-11d which was cut transverse to the growth axis and has different distances) that would be similar to a bulk drilling method. Error bars on "bulk" calculations represent standard deviation or each slice (or distance from the tip). The "bulk" values from each slice and/or distance do not vary along the growth axis, especially relative to the variability observed in each slice (see Fig. 3).

3.2 Deviations from equilibrium with seawater $\delta^{18}O$ and $\delta^{13}C$

To determine where the corals record isotopic compositions closest to an environmental signal, we calculated carbonate isotopic equilibrium values using data reported for nearby hydrographic stations. The seawater stable isotope ratios and temperature were determined using the average composition of the 490–650 m depth range (similar to the coral collection depths; Table S2 in the Supplement) at stations nearest the coral dredge sites (Fig. 1). For seawater $\delta^{18}O$, we gathered seawater temperature, potential temperature, and salinity records from CTD cast data from the AnSlope (Cross-slope exchanges at the Antarctic Slope Front) project that sampled very close to our dredge sites (Fig. 1 and Fig. S2 in the Supplement) (Jacobs, 2015; Visbeck, 2015; Gordon, 2016). The average potential temperature (-0.12 ± 0.09° C) and salinity (34.7 ± 0.002) were used to identify the water mass at our locale and depth as Low Salinity Bottom Water, as described by Jacobs et al. (1985; Table S2 in the Supplement). The reported $\delta^{18}O$ for this water mass is -0.26 ± 0.06 ‰ (Jacobs et al., 1985). With the seawater $\delta^{18}O$ and average seawater temperature within our depth range, we calculated the equilibrium carbonate $\delta^{18}O$ value as 3.66 ± 0.06 ‰ for calcite and 4.51 ± 0.06 ‰ for aragonite using equations from O'Neil et al. (1969) and Grossman and Ku (1986), respectively. Determining seawater $\delta^{13}C$ was straightforward

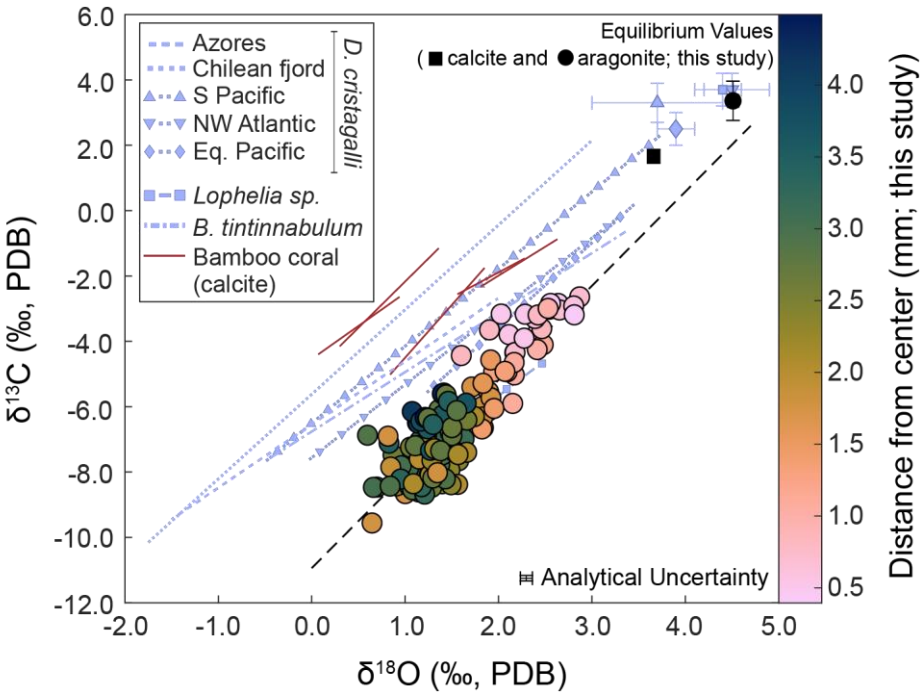

Figure 5: Linear regressions of $\delta^{18}O$ vs $\delta^{13}C$ values for *E. fissurata* (colored circles and black dashed line) compared to scleractinian and bamboo corals (purple and red lines, respectively). Lines for external data are not extrapolated beyond the range of reported $\delta^{18}O$ values. Color of circles corresponds to distance from the coral center, see color bar at the right. Calculated equilibrium values for *E. fissurata* are also shown as black square (relative to calcite) and circle (relative to aragonite). The dashed black line represents the line of best fit for the measured values ($\delta^{13}C$ = 2.88 (±0.14) * $\delta^{18}O$-10.94 (±0.22)). Linear regressions for *D. cristagalli* and *Lophelia sp.* are reported by Adkins et al. (2003) and the dashed lines with shapes have corresponding equilibria displayed (matching shape with error bars). Each *D. cristagalli* specimen is labelled by its locale and the *Lophelia* specimen was recovered from the NE Atlantic. The *B. tintinnabulum* was recovered from the Blake Plateau and data are reported by Emiliani et al. (1978). Bamboo coral data are from Hill et al. (2011) collected from the California margin. The slope of the linear regression produced in this study is similar to those reported for other deep-sea corals, with a similar decrease in both isotopic ratios. Additionally, the measured values closest to equilibria are those toward the center of each coral disc, as noted by the lighter colors.

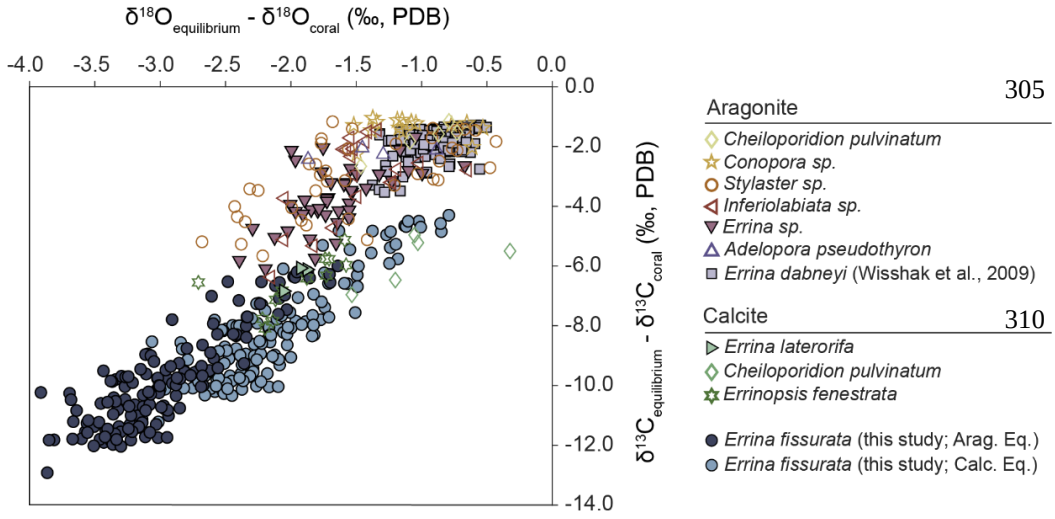

Figure 6: Difference between measured coral isotope ratios and equilibrium values for compilation of stylasterid corals. Except for *E. dabneyi* and *E. fissurata*, all coral isotope data are from Samperiz et al. (2020) and the corresponding equilibrium values were calculated using corresponding seawater data from Samperiz et al. and equations from Grossman and Ku (1986; aragonite $\delta^{18}O$ equilibrium), O'Neil et al. (1969; calcite $\delta^{18}O$ equilibrium), and Romanek et al. (1992; aragonite and calcite $\delta^{13}C$ equilibrium). *Errina dabneyi* data and $\delta^{18}O$ equilibrium are from Wisshak et al. (2009), and the $\delta^{13}C$ equilibrium was calculated using reported seawater data from Wisshak et al. (2010). Filled symbols represent all *Errina* specimens. The corals from this study exhibit a similar offset from equilibrium to other calcitic specimens. Some of the values closer to equilibrium (relative to calcite) from the *E. fissurata*, even overlap with aragonitic samples as well. Note that stylasterid data shown in Figure 6 are included here.

as direct measurements existed for nearby WOCE (World Ocean Circulation Experiment) stations (Fig. 1 and Fig. S2 in the Supplement) (WOCE, 2002). Using the average of reported seawater $\delta^{13}C$ values for our depth range (0.66 ± 0.05 ‰), we calculated equilibrium carbonate $\delta^{13}C$ values as 1.66 ± 0.20 ‰ for calcite and 3.36 ± 0.60 ‰ for aragonite with equations from Romanek et al. (1992) (Fig. 5; Table S2 in the Supplement).We calculated equilibrium values for both calcite and aragonite because stylasterids have exhibited mixed mineralogy, and we have evidence for that here (Cairns and Macintyre, 1992; Sect. 4.2.3).

Each coral slice exhibits a significant offset from the calculated equilibrium values, the smallest offsets located in the center of each coral slice (Figs. 5, 6, and 7). These equilibrium offsets are all negative in direction (i.e., the corals record isotopic ratios less than expected equilibrium) and range from -3.91 to -0.79 ‰ for $\delta^{18}O$ and from -12.92 to -4.30 ‰ for $\delta^{13}C$. The offsets from $\delta^{13}C$ equilibrium are consistently larger than those of $\delta^{18}O$, and the offsets relative to aragonite equilibrium are larger than those calculated relative to calcite equilibrium (Fig. 6). Additionally, we observe a strong linear correlation between $\delta^{18}O$ and $\delta^{13}C$ values. The compilation of samples in this study result in a linear trend with a slope of 2.88 ± 0.14 ($\Delta\delta^{13}C/\Delta\delta^{18}O$; R^2=0.76) or 0.26 ±0.01 ($\Delta\delta^{18}O/\Delta\delta^{13}C$; R^2=0.76) that passes near the calculated equilibrium values (Fig. 5 and Table 2). Most noticeable is that the values measured from closest to the center of the coral slice are consistently closest to calculated equilibrium, whereas the values from the mid to outer sections are further from equilibrium (Fig. 5).

4 Discussion

4.1 Evaluation of major $\delta^{18}O$ and $\delta^{13}C$ trends

Regarding large-scale isotopic trends from the tip to the base of each coral specimen, our results do not directly support those of Samperiz et al. (2020). In their work, Samperiz et al. observed significant differences among stable isotopic compositions of carbonate sampled from different portions of a single specimen. Samples drilled from the main trunk and secondary branches exhibited higher $\delta^{18}O$ and $\delta^{13}C$ values (which were closer to seawater equilibrium) than the more distal growth tips. An observation evident in not only different genera of stylasterid corals, but also between calcite and aragonite mineralogies (Samperiz et al., 2020). Here, specimen EA-11 supported this observation as the most negative $\delta^{18}O$ and $\delta^{13}C$ values were measured on the slice closest to the tip, EA-11a, and the most positive $\delta^{18}O$ and $\delta^{13}C$ values were measured on a slice furthest from the tip, EA-11d (Fig. 4). Specimen EA-12 was characterized by $\delta^{18}O$ and $\delta^{13}C$ minima nearest the tip (EA-11a), but the maximum isotope ratios were measured on different slices: the most positive $\delta^{18}O$ was closer to the tip and the most positive $\delta^{13}C$ was further away (Fig. 4 and Table 2). These results neither completely support nor refute those of Samperiz et al. (2020). We posit that our sampling scheme hindered a full support from both corals analyzed here. For EA-12, we did not sample the main coral trunk, but rather just above it, targeting a region that exhibited

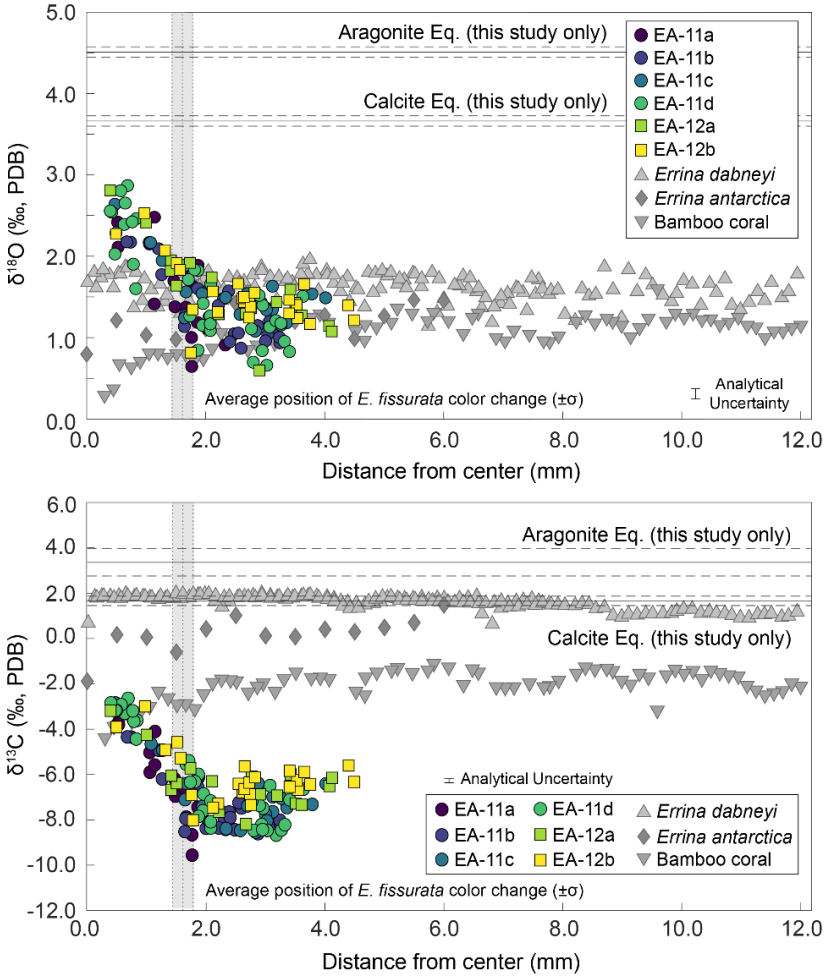

Figure 7: Oxygen (top) and carbon (bottom) stable isotope ratios by distance from the center of the coral. The values from this study are plotted by slice from each specimen as noted by the colored circles (EA-11) and squares (EA-12). The horizontal lines denote calculated aragonite and calcite equilibrium values for this study with corresponding uncertainty in dashed lines (±1σ). Vertical gray bars denote the average radius of the white coral center for *E. fissurata*, the width of the bar denoting ±1σ. Also included are additional coral data sampled in a similar transect style. *E. dabneyi* is from Wishhak et al. (2009), *E. antarctica* is from Samperiz et al. (2020), and the bamboo coral data are from Hill et al. (2011). Regarding $\delta^{18}O$, the *E. antarctica* and bamboo coral seem to have a small decrease in the last few datapoints toward the center. Regarding $\delta^{13}C$, the same is true of each of the corals from other studies. This is opposite of what we observe in our corals. We also note a much larger magnitude of change across the transect with no observable trend among coral slices (i.e., by distance from the coral tip), only the increase in isotopic values toward the white, center region of the corals.

isotopic variability in the corals from Samperiz et al. (2020) (Fig. 2). The sampling scheme here was designed to exploit any isotopic variability across a coral slice, thus considering the "bulk" values from each slice should provide a more comparable sampling strategy to Samperiz et al. (2020). However, our calculated bulk values do not exhibit any significant changes over the lengths of the corals (Fig. 4). This could be because we did not sample the true tips of the corals, but instead were ~1 cm below, possibly preventing us from sampling the most negative $\delta^{18}O$ and $\delta^{13}C$. We are also uncertain of the lower extent of EA-11 and EA-12, as they were dredge collected, and could be missing a portion of the main trunk, possibly preventing us from sampling the most positive $\delta^{18}O$ and $\delta^{13}C$ (Fig. 2).

Another isotopic trend we consider here is that of the linear correlation between $\delta^{18}O$ and $\delta^{13}C$ values. Because these corals are living animals, and their biological functions affect the carbon and oxygen pools from which they calcify, we anticipated that the resulting $\delta^{18}O$ and $\delta^{13}C$ records would be positively correlated and offset to more negative values than calculated equilibrium (Emiliani et al., 1978; Swart, 1983; McConnaughey, 1989a; Smith et al., 2000; Adkins et al., 2003; Hill et al., 2011; Samperiz et al., 2020; Stewart et al., 2020). In Figure 5, we compare the data from this study with several scleractinian and bamboo corals (class Anthozoa). Our data exhibit very similar slopes to other deep-sea corals and fall within similar ranges of isotopic compositions. This supports that vital effects can have a similar influence on corals of different classes, and across different latitudinal and depth ranges. We also compare our corals to the deep-sea stylasterids compiled by Samperiz et al. (2020) and Wisshak et al. (2009) (Fig. 6). Samperiz et al. (2020) observed that calcitic specimens exhibited $\delta^{18}O$ and $\delta^{13}C$ values further from equilibrium (i.e., more negative) compared to aragonitic corals. Because our calculated equilibrium $\delta^{18}O$ and $\delta^{13}C$ values were higher for aragonite than calcite, our data relative to aragonite equilibrium are further offset, contradicting the observation made by Samperiz et al. (2020). However, our data relative to calcite equilibrium exhibit overlaps with both calcitic specimens and some aragonite *Errina* data points as well (Fig. 6, Sect. 4.2.3). Thus far our data fit in well with established $\delta^{18}O$ and $\delta^{13}C$ records from other deep-sea stylasterids, scleractinians, and bamboo corals. Our data are distinguished when we examine the heterogeneous $\delta^{18}O$ and $\delta^{13}C$ values across a coral slice.

We compare our $\delta^{18}O$ and $\delta^{13}C$ results to those of other azooxanthellate, deep-sea stylasterid and bamboo corals sampled in a similar manner, i.e., across growth bands, perpendicular to the growth axis. The range of $\delta^{18}O$ values for EA-11 and EA-12 is 2.27 ‰, larger than the range for the *E. dabneyi* (~0.8 ‰; Wisshak et al., 2009), *E. antarctica* (~0.6 ‰; Samperiz et al., 2020), and the bamboo coral (~1 ‰; Hill et al., 2011) (Fig. 7). Similarly, greater heterogeneity is evident in the range of $\delta^{13}C$ values exhibited by EA-11 and EA-12 (6.92 ‰) compared to *E. dabneyi* (~1.4 ‰), *E. antarctica* (~3 ‰), and the bamboo coral (~3.5 ‰) (Fig. 7). This contradicts results of Stewart et al. (2020) wherein the authors find that stylasterid corals of mixed mineralogy exhibit less variability compared to purely aragonitic scleractinians and stylasterids. We have evidence for a mixed calcite and aragonite mineralogy in the corals presented here (Sect. 4.2.3), but they are characterized by the largest stable isotope variability. This could be an artifact of sampling scheme between our study and Stewart et al. (2020), as our method was designed to amplify spatial variability in stable isotopic compositions across the coral slices. The increased internal variability

could also be a species-specific effect such that the calcification pattern for *E. fissurata* imparts stronger vital effects in the mid to outer coral regions compared to center. Spatially variable vital effects have been observed in many deep-sea corals, and departures of at least 2 ‰ in $\delta^{18}O$ have been recorded by *D. cristagalli* (Smith et al., 2002; Adkins et al., 2003). To test if the $\delta^{18}O$ variability in our corals represents an environmental signal, we use the stylasterid temperature calibration from Samperiz et al. (2020) and calculate the temperature change to be up to ~7° C across each coral slice and ~10° C along the vertical section of EA-11d. Such temperature changes are too large for the western Ross Sea over the lifespan of a single coral specimen (estimated to be ~200–400 years based on growth rate estimates for this species by King et al. (2018)). In Figure 7, we are also able to compare the trends of our $\delta^{18}O$ and $\delta^{13}C$ values to those of *E. dabneyi*, *E. antarctica*, and bamboo coral specimens across their surfaces, perpendicular to the growth axis. Our stylasterids demonstrate a very clear and large-magnitude shift to higher $\delta^{18}O$ and $\delta^{13}C$ values toward the center of the coral slice (Fig. 7). This is opposite to the trend exhibited by the *E. antarctica* and bamboo coral $\delta^{18}O$ values, and all three corals' $\delta^{13}C$ values. Because the three external corals were sampled following visual growth banding, we posit that there is a difference between the two main growth styles (calcification) that cause the disparity in the central $\delta^{18}O$ and $\delta^{13}C$ values related to vital effects.

4.2 Surveying maps of skeletal stable isotope composition: alternative mechanisms for high central $\delta^{18}O$ and $\delta^{13}C$ values

4.2.1 Organic contribution to outer skeletal portion

Stylasterid corals have been observed hosting other species including boring cyanobacteria, sponges, and gastropods, all of which could affect the isotopic composition of the coral skeleton (Puce et al., 2009; Braga-Henriques et al., 2010; Pica et al., 2015). The presence of symbionts could contribute metabolic carbon and/or oxygen to the pool from which the corals calcify. Depending on the relationship of the symbiont, and if it is living near an active calcification site, isotopically light metabolic products could be incorporated into the coral carbonate, driving the outer portions of the coral to lower $\delta^{18}O$ and $\delta^{13}C$ (Epstein et al., 1951). There have been direct observations of barnacles living on *E. fissurata* (Pica et al., 2015). For specimen EA-11, sections with any obvious external growth or signs of hosting were avoided and only clean slices were selected for sampling. For EA-12, however, this coral was believed to be dead upon collection, and covered in possible organic growth/encrustation over time (Fig. 2). We posit that this material was not present at the time of coral calcification and therefore would not have altered the $\delta^{18}O$ and $\delta^{13}C$ values of the carbonate. The similarity in isotope trends between both specimens supports this hypothesis.

4.2.2 Diagenetic influence on stable isotopic composition

Coral diagenesis can be described as a post-calcification alteration of carbonate geochemistry. Such processes could directly change the skeletal $\delta^{18}O$ and $\delta^{13}C$ values by removing or replacing the carbonate. Identifiable diagenetic features for stylasterid corals have been described by Black and Andrus (2009), including encrustation of foreign materials on the outer surface of the coral skeleton, microspar fabric and microbioclastic debris, abrasions, fragmentation, pitting, and bioerosion. These features

are identifiable via scanning electron microscopy (SEM), but the authors found no impact on the $\delta^{18}O$ and $\delta^{13}C$ after analyzing fossil and modern corals (Black and Andrus, 2009). Work by Wisshak et al. (2009) has identified additional diagenetic impacts on stylasterid corals via micro-scale dissolution and re-precipitation. We did not image specimens EA-11 or EA-12 via SEM, but we were able to image other specimens collected from the same dredges. We did not see any signs of the diagenetic effects described, except for possible secondary growth or recrystallization (Fig. S3 in the Supplement). Although we have identified evidence of secondary crystal growth, the scale is on the order of ~100 μm. That size is 5 times smaller than the size of the drill bit used here, and therefore unlikely to have an impact on the $\delta^{18}O$ and $\delta^{13}C$ variability observed.

4.2.3 Calcite versus aragonite mineralogy

Stylasterid corals have been shown to precipitate their skeletons from calcite, aragonite, a
nd both coexisting polymorphs (Cairns and Macintyre, 1992). Calcitic stylasterid corals have demonstrated significantly lower $\delta^{18}O$ and $\delta^{13}C$ values than aragonite stylasterids (Samperiz et al., 2020). As mentioned in a previous section, stylasterids have also exhibited different levels of $\delta^{18}O$ and $\delta^{13}C$ variability within a single coral based on mineralogy (Stewart et al., 2020). Thus, mineralogy will have a significant impact on stable isotopic composition. The specimens in this study were not used for mineralogical analysis, but corals from the same dredges were. Using both XRD and false-color imaging methods, we have identified that these corals are likely mixed mineralogy, and mostly calcitic (Table 3 and Fig. S4 in the Supplement). Two corals were sampled (one modern and one dead) from both the center white, and outer pink regions. Each coral sample produced similar results of ~75 % calcite, and ~25 % aragonite (Table 3). We consider that there is a small change in the percentage of calcite from the outer portions of both corals (75 % to 80 %) compared to the inner portions (70 % to77 %). However, the changes are small, and we posit that although calcitic stylasterids demonstrate lower skeletal $\delta^{18}O$ and $\delta^{13}C$ values compared to aragonite, the mineralogical difference is likely not enough to be driving the $\delta^{18}O$ and $\delta^{13}C$ patterns here (Fig. 3).

Coral	Sample Location	Aragonite	Calcite
Modern	Center	23%	77%
	External	20%	80%
Dead	Center	30%	70%
	External	25%	75%

Table 3: Results for XRD mineralogical analysis.

4.3 Hypothesized large-scale calcification model for *E. fissurata*

The most parsimonious explanation for the specimen-scale differences in $\delta^{18}O$ and $\delta^{13}C$ values is that the coral calcifies in a way that magnifies the vital effects in the outer region compared to the center. In order to grow dendritically, the most intuitive growth model for corals such as our stylasterids holds that the center of each branch extends axially faster than each branch thickens radially. Thus, the kinetic effects would be most apparent in the center of each coral slice and lessen towards the outer edges, resulting in $\delta^{18}O$ and $\delta^{13}C$ values that would therefore approach equilibrium toward the edges of each isotope map. Many marine calcifying organisms (e.g., mollusks and corals) follow the Von Bertalanaffy growth model wherein their calcification rate ontogenetically decreases, and we posited that this model also applied to the horizontal extension of

stylasterids as they prioritize vertical growth (Ralph and Maxwell, 1977; Emiliani et al., 1978; Berkman, 1990; Philipp et al., 2005; Román-González et al., 2017). Such a coral growth model is supported by observations from Fallon et al. (2014) wherein a cold water scleractinian coral demonstrated growth similar to stacking cones with a fast growing tip. This structure is also supported by isotopic records of other stylasterids and bamboo corals which were all characterized by low isotopic values at the regions of most rapid growth (Wisshak et al., 2009; Samperiz et al., 2020; Hill et al., 2011).

To better understand our resulting trends, we created models that reflect simplified calcification scenarios of constant, decreasing, and increasing radial extension with time. The model calculations were based on an idealized coral slice of n rings with radii, r_{n+1}, an initial growth inner circle of radius, r_1, and the extension rate represented by the change in radius, Δr, between each ring (Fig. 8). We set each model to run for 100 years and examined the rate of change of coral area as a proxy for calcification rate in each scenario. Whereas few studies have determined vertical growth rates of deep-sea stylasterid corals (Stratford et al., 2001; Chong and Stratford, 2002; Miller et al., 2004; Wisshak et al., 2009; King et al., 2018), their radial extension rates remain largely unknown. Therefore, we employed a range of radial growth rates reported for live-collected bamboo corals living at a depth of 1000–1700 m (Thresher et al., 2011). The bamboo corals were reported to grow from 0.01–0.12 mm y^{-1}; therefore, our constant radial extension scenario was characterized by the median 0.065 mm y^{-1} (Fig. 9a–c). The decreasing radial extension scenario was initially set to the maximum extension rate of 0.12 mm y^{-1} that decreased linearly by 0.0011 mm y^{-2} until the minimum growth rate of 0.01 mm y^{-1} was reached at 100 years (Fig. 9d–f). For the increasing radial extension scenario, the opposite was set, an initial radial extension rate of the minimum 0.01 mm y^{-1} and a linear increase at a rate of 0.0011 mm y^{-2} until 0.12 mm y^{-1} at 100 years (Fig. 9g–i).

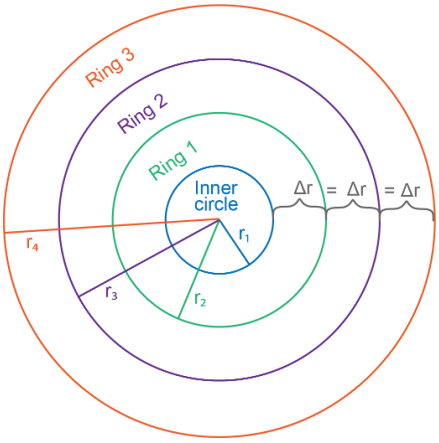

Figure 8: Coral slice schematic used for calcification models. In this simplified model, growth begins with the inner circle of radius r_1. Each growth increment is noted by a new ring, Ring n, with a radius, r_{n+1}. In this case, the change in radius between each ring, Δr, is equal representing the constant radial extension model. The Δr becomes larger or smaller with each ring for the increasing and degreasing growth scenarios, respectively.

We observe stronger vital effects toward the outer edges of the coral surfaces and interpret this as increased calcification rate along the outer edges. To test if this growth scenario likely represents our stable isotope maps, we defined changes in calcification rate as the two-dimensional changes in coral area with time. We then compared the resulting models to the changes in stable isotope values across each coral slice (assuming no change in the ambient seawater values during the time of precipitation). In the case of the constant radial extension, the growth rings are evenly spaced, leading to a steady increase of horizontal area between the rings with time (Fig. 9a and b). Constant radial extension refers to constant change in area with time (Fig. 9c). Such a growth model would result in stable isotope values to either be constant across the surface of the coral

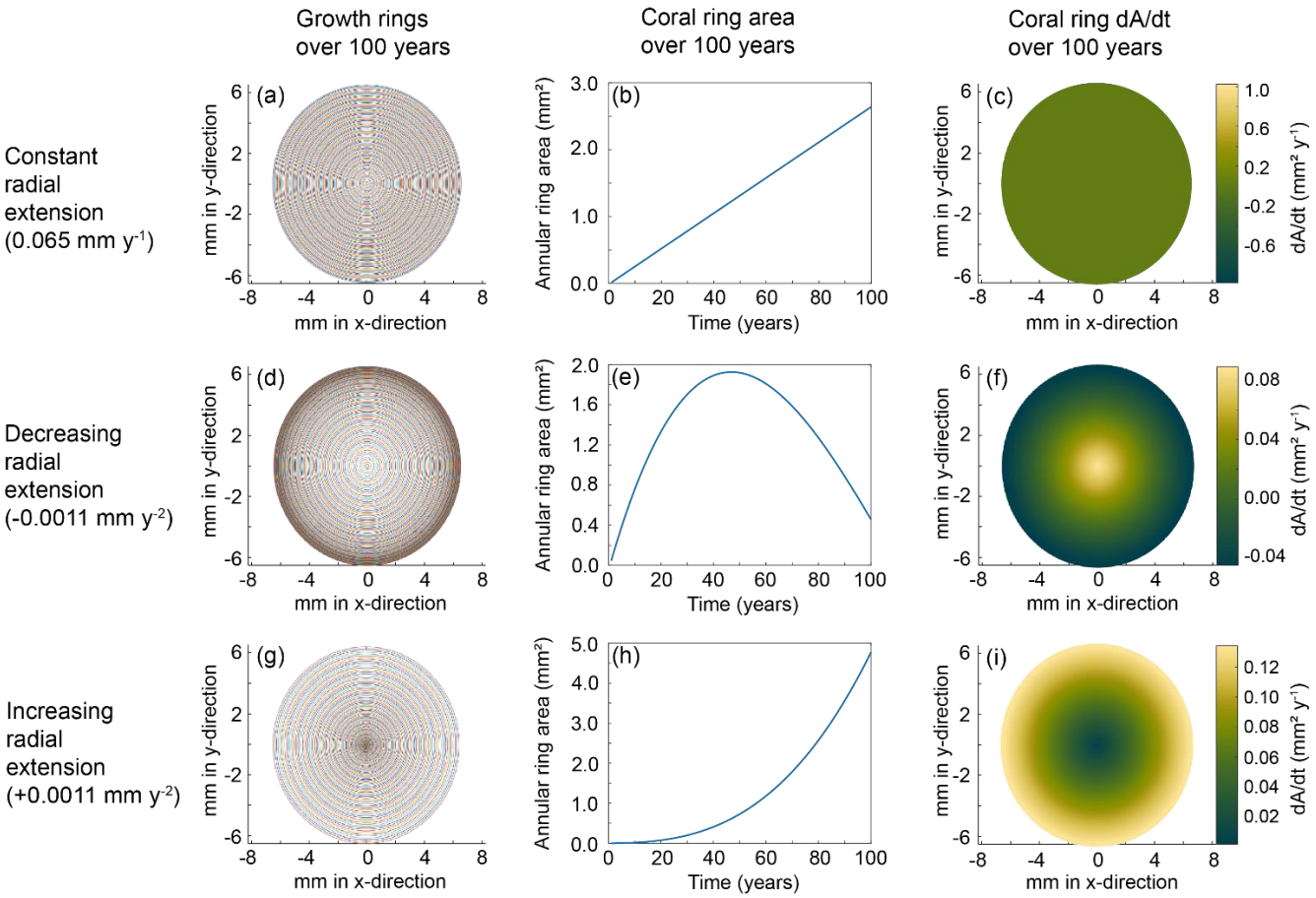

Figure 9: Coral calcification models for each scenario. The top row (a–c) depicts results from the constant radial extension model, the middle row (d–f) is the decreasing radial extension, and the bottom row (g–i) is the increasing radial extension model. The left column depicts the growth rings for each model after a run of 100 years. The middle column shows the change in area with each year of calcification. The right column shows the rate of change in coral area for each model. The corresponding color bars represent the magnitude of change.

or record any changes that reflect seawater variability. Decreasing radial extension with time relates to decreasing area with time (Fig. 9d–f). We hypothesized decreasing radial extension to be the most likely calcification pattern as the available literature supports slowing growth with time among marine carbonates (Ralph and Maxwell, 1977; Emiliani et al., 1978; Berkman, 1990; Philipp et al., 2005; Román-González et al., 2017). With a decreasing radial extension, the growth bands become closer with time, causing the area to increase then decrease over the modeled 100-year span (Fig. 9d and e). Therefore, the rate of change of area decreases toward the outer edges of the coral surface (Fig. 9f). Because faster calcification results in stronger vital effects, the center of the coral would exhibit isotope values furthest from equilibrium. That is the opposite of what we observed. The increasing radial extension scenario led to growth bands increasing distance from each other, resulting in an exponential increase in area (Fig. 9g and h). The resulting calcification scheme (i.e., rate of change in area) would lead

to stronger vital effects toward the outer edges of the coral surface and isotopic values closer to equilibrium in the center (Fig. 9i). This is what we observed.

The unique pattern of the highest isotopic values in the center of the coral with lower values toward the mid and outer edge rejects our hypothesis for calcification and is contradicted by previously published isotope records and growth models. The stable isotope maps instead support rapid calcification toward the outer region and slow calcification in the center. Such a model, however, is not supported by previously mentioned growth habits of marine carbonates and would not result in dendritic corals. Several studies involving scleractinian corals and octocorals (class Anthozoa whereas stylasterids are class Hydrozoa) have converged on similar two-stage calcification patterns. Using X-ray micro-computed tomography, Urushihara et al. (2016) were able to determine that the cold water octocoral, *Corallium konojoi* (~290 m water depth), calcifies by two processes: formation of sclerites (small aggregates of carbonate within the coenenchyme tissue surrounding polyps) and a combined sclerite/biomineralization process at the apical region where skeletogenic epithelium secretes carbonate. A similar growth strategy was observed using incubated octocorals, *Corallium rubrum* (~20 m water depth), and measuring uptake of isotopic tracers (Allemand and Benazet-Tambutte, 1996). The authors found that the red coral forms its axial skeleton via biomineralization from the skeletogenic epithelium, which contributes to its horizontal extension. At the apical region, spicules fuse with the skeleton for vertical extension (Allemand and Benazet-Tambutte, 1996). Additional isotopic labeling experiments involving the zooxanthellate scleractinian, *Porites porites* (~50 m water depth), identified "hot spots" of calcification wherein biomineralization was not uniform across the growing surface of the coral (Houlbrèque et al., 2009). The authors attributed the heterogeneous calcification to an uneven distribution of extracellular calcifying fluid within the coral (Houlbrèque et al., 2009). The scleractinian calcification patterns described here are not a direct analog for our *E. fissurata* growth, however, a calcification strategy that invokes uneven, or two-step biomineralization could account for the spatial distribution of vital effects observed in our coral isotope maps.

A growth model of shallow water staghorn coral (*Acropora cervicornis*) over daily to yearly timescales best reconciles our data (Gladfelter 1982, 1983, 1984). The Gladfelter model includes two main phases: rapid extension by randomly oriented crystals that develop the main skeletal framework, followed by infilling and strengthening of the skeleton along the entire growth axis (Gladfelter, 1982). Gladfelter (1983) observed that the initial framework growth was largely around the mid and outer regions of the corallite and the infilling occurred later in the center. We posit that the basic premise of this model (rapid initial growth followed by slower calcification) describes the coral growth presented here. The lower isotopic values toward the outer edge signify enhanced kinetic fractionation from the rapid growth. The center region of the coral calcifies at a slower rate; thus, kinetic fractionation is reduced resulting in higher isotopic values closer to equilibrium. We acknowledge that the Gladfelter growth model employs fusiform crystals setting a foundation upon which bundles of aragonite crystals grow, and we do not suggest that the same crystal structures are apparent here. We instead hypothesize that because of our consistent spatial isotopic discrepancies, and our contrast to previous stylasterid works, there must be a heterogeneous growth structure

for *E. fissurata* not previously described for stylasterids. Our unique sampling scheme allowed for the resolution necessary to improve our understanding of the formation of a valuable paleoceanographic archive.

4.4 Considerations for paleoceanographic reconstructions

The definitive trend of increasing isotopic values toward the inner, white section of the coral supports that this is the ideal region of the coral from which to sample *E. fissurata* for paleotemperature reconstructions. Because the higher values are located nearest the white section of the coral and not the geometric center, we converted the images of each slice to grayscale (Fig. 10). This allowed us to find the whitest pixels and quantitatively determine the most ideal location for sampling. With the exception of the light outer edges, the sample holes that were at least 75 % surrounded by the whitest pixels were selected for temperature reconstructions (Fig. 10). These $\delta^{18}O$ values were averaged for each coral slice and were used with the stylasterid temperature calibration from Samperiz et al. (2020). Additionally, the $\delta^{18}O$ average for each entire slice was calculated to determine a "bulk" value that would represent a common sampling method of drilling across the growth axis. The bulk $\delta^{18}O$ values were also calibrated to temperature and the results are illustrated in Fig. 10 (Table S3 in the Supplement). Note that for slice EA-11d that consists of a vertical face rather than horizontal, $\delta^{18}O$ values were only combined for the same distance from the coral tip.

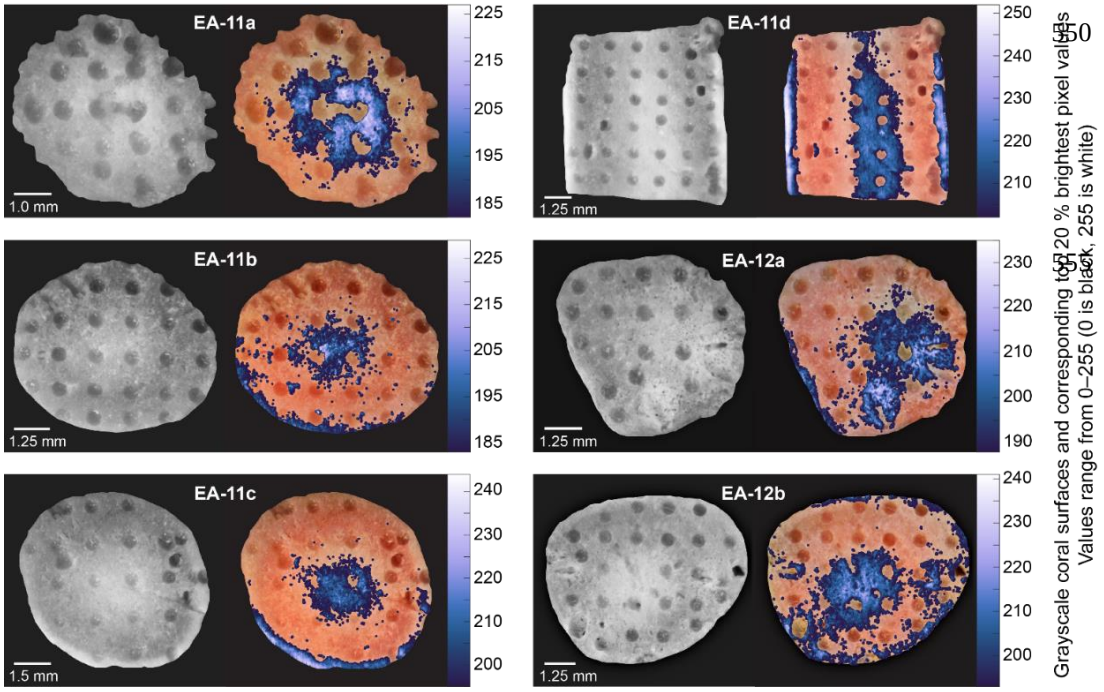

Figure 10: Compilation of grayscale images and corresponding brightest pixels (highest 20 %) over each coral slice. The colors correspond to the grayscale pixel value (higher on the scale bar denotes a whiter pixel). The sample holes surrounded by at least ~75 % of bright pixels were used to calculate representative $\delta^{18}O$ values for each slice for temperature calibration (Table S3 in the Supplement).

Although both the "central" and "bulk" temperature records are higher than current ocean temperatures of a similar depth, the center values are significantly different from bulk

measurements and are closer to the true environmental signal (Fig. 11). We compared the center and bulk temperature records using the Student's t-Test to determine whether the difference between the means is significant or occurred by chance (from variability). We used a paired t-Test to compare center and bulk temperatures from the same distance from the tip where available. With a p-value of 6.61×10^{-6}, the difference between center and bulk temperatures is very unlikely to have occurred by chance (Table S4 in the Supplement). This analysis, however, assumes no environmental change over the lifespan of the corals. To account for possible seawater changes and more accurately reflect the samples that would be targeted for temperature reconstructions, we also tested individual temperatures across each slice (rather than the averages used in Fig. 11). The unpaired t-Test required at least two temperature values that were sampled from the white center and the pink outer regions for at least one degree of freedom. This was met by four coral slices, EA-11a, EA-11b, EA-11d (63.55 mm from the tip), and EA-12b; each test producing p-values less than 0.005 (Table S4 in the Supplement). These analyses show that we can conceive of no comparison within coral slices that show the same values between the center and bulk temperatures.

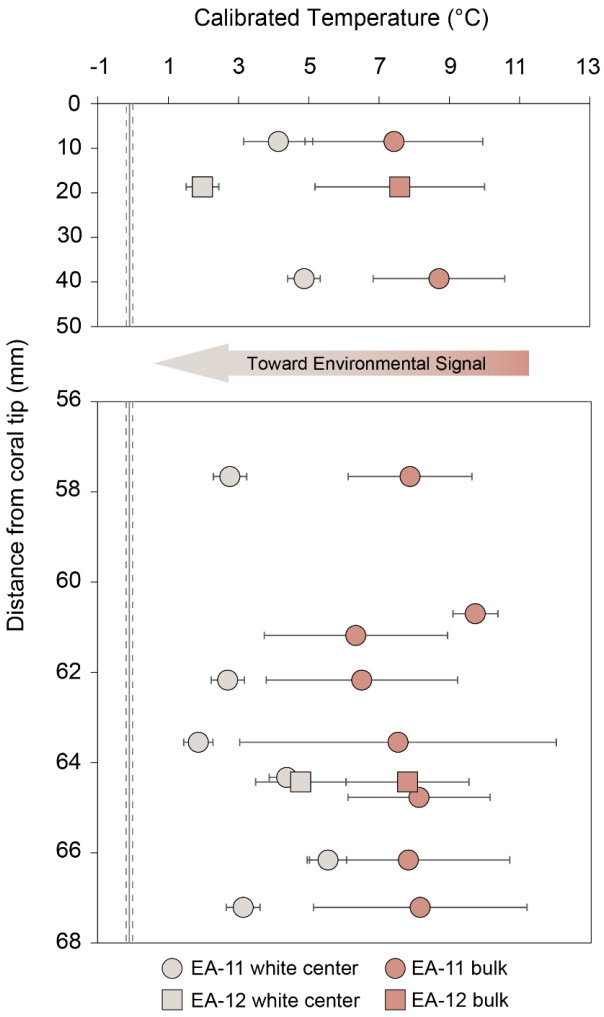

Figure 11: Temperature calibration using the equation from Samperiz et al. (2020). Light colored points denote temperatures using the $\delta^{18}O$ values from the white centers of each slice, whereas the darker, peach color denote a "bulk" measurement. The bulk is calculated using the average $\delta^{18}O$ of the entire slice, similar to a value that would be measured from a sample collected via drilling into the side of a coral specimen. Error bars are based on standard deviation of three or more averaged samples. The error bars for less than three samples are based on the analytical error propagation (Table S3 in the Supplement).

Figure 11 shows that detailed analysis of isotopic distributions through *E. fissurata* skeletons does not quite achieve samples representative of isotope equilibrium; but closer approach is possible. With the aid of computerized tomography (CT) scanning methods, perhaps density banding skeletal structures could be visualized, enabling even finer-scale samples . We posit that our prescribed sampling scheme for these corals, paired with CT-guided sampling, can yield robust paleotemperature records. Sampled as we have, with even distribution of samples over the surface of each disc as a goal, our reconstructed temperatures are higher than a likely environmental signal (Fig. 11). However, we have demonstrated that the center white region of these corals is less affected by vital effects and less likely altered after

initial deposition. Therefore, we recommend sampling of the white center using more spatially precise micro-milling methods to target even smaller regions, thus minimizing the impact of vital effects. We also note that in calculating uncertainty associated with temperature calibrations, our center temperature errors are likely underestimated as they rely largely on analytical uncertainty. However, our calculation of temperatures from bulk data includes high spatial standard deviations; more precise sampling would yield more precise temperature estimates. Thus, a targeted milling approach would likely reflect a more accurate uncertainty estimate on the temperature as well. Additionally, CT scanning that reveals coral growth structures, such as Puce et al. (2011), would allow an even closer approach to accurate paleoceanographic reconstructions. Such combined methods would allow for extremely targeted sampling considering both the growth structure and biomineralization methods to inform sampling efforts to allow closer approach to equilibrium and better accuracy of paleotemperature reconstructions using *Errina* corals.

5 Conclusions

The results presented here provide the paleoceanographic community with a new understanding of the influence of vital effects on coral paleo-archives. We have demonstrated that deep-sea stylasterid corals exhibit significant and variable vital effects between different taxa that obscure the environmental signal. In the case of E. fissurata, we are also able to provide and interpret isotope maps that guide future coral sampling efforts. Lacking any visible banding structure, the specimens in this study benefitted from a gridded sampling scheme to determine the location of minimum influence from vital effects. Our skeletal $\delta^{18}O$ and $\delta^{13}C$ values exhibit an increasing trend toward seawater equilibrium near the center of the coral. This result contradicts growth structures hypothesized in the current body of literature based on observed stable isotopic trends (Wisshak et al., 2009; Samperiz et al., 2020; Hill et al., 2011), but supports a two-stage growth model that describes a "hasty" initial lattice framework construction, followed by slower infilling to strengthen, and support the coral colony (Gladfelter, 1982, 1983). The samples from the center white region of the corals produced temperature records significantly different than a bulk approach and were closest to nearby ocean temperatures. Thus, we recommend sampling this taxon along the center, white region where the carbonate geochemical record is closest to seawater equilibrium and an environmental isotopic signal. Further, we suggest initial CT scanning of corals to determine any hidden growth features, and micro milling sampling techniques to target the location of the most accurate record. Combined with a new stylasterid temperature calibration (Samperiz et al., 2020), we posit that accurate paleotemperature records can be reconstructed from deep-sea *Errina fissurata* corals.

Data availability

All data are available in the supplement.

Author contributions

TMK and BER contributed to the conceptualization of the work. TMK developed sampling methods under the supervision of BER. All authors contributed to formal analysis. TMK wrote the manuscript draft, with significant input from BER. All authors approved the final version of the manuscript.

Competing interests

The authors declare that they have no conflict of interest.

Acknowledgements

We thank the captain, crew, and scientific staff of the RV *Nathaniel B. Palmer* during the US Antarctic Program expedition NBP07-01 to the Ross Sea, Antarctica for their efforts in coral collection. We also thank Dr. Ernst Peebles for the use of laboratory space during coral sampling, and Drs. Jennifer Granneman and David Jones for guidance on both slicing the corals and initial setup of the MircoMill. During this project, TMK was funded through the Genshaft Family Dissertation Fellowship awarded by the University of South Florida as well as three endowed fellowships from the College of Marine Science: Carl Riggs Endowed Fellowship, George Lorton Fellowship in Marine Science, and the Abby Sallenger Memorial Award.

References

Adkins, J. F., Cheng, H., Boyle, E. A., Druffel, E. R. M., and Edwards, R. L.: Deep-Sea Coral Evidence for Rapid Change in Ventilation of the Deep North Atlantic 15,400 Years Ago, Science, 280, 725–728, https://doi.org/10.1126/science.280.5364.725, 1998.

Adkins, J. F., Boyle, E. A., Curry, W. B., and Lutringer, A.: Stable isotopes in deep-sea corals and a new mechanism for "vital effects," Geochim. Cosmochim. Ac., 67, 1129–1143, https://doi.org/10.1016/S0016-7037(02)01203-6, 2003.

Allemand, D. and Benazet-Tambutte, S.: Dynamics of calcification in the mediterranean red coral, Corallium rubrum (Linnaeus) (Cnidaria, Octocorallia), J. Exp. Zool., 276, 270–278, https://doi.org/10.1002/(SICI)1097-010X(19961101)276:4<270::AID-JEZ4>3.0.CO;2-L, 1996.

Andrews, A. H., Cordes, E. E., Mahoney, M. M., Munk, K., Coale, K. H., Cailliet, G. M., and Heifetz, J.: Age, growth and radiometric age validation of a deep-sea, habitat-forming gorgonian (Primnoa resedaeformis) from the Gulf of Alaska, Hydrobiologia, 471, 101–110, https://doi.org/10.1023/A:1016501320206, 2002.

Arndt, J. E., Schenke, H. W., Jakobsson, M., Nitsche, F. O., Buys, G., Goleby, B., Rebesco, M., Bohoyo, F., Hong, J., Black, J., Greku, R., Udintsev, G., Barrios, F., Reynoso-Peralta, W., Taisei, M., and Wigley, R.: The International Bathymetric Chart of the Southern Ocean (IBCSO) Version 1.0-A new bathymetric compilation covering circum-Antarctic waters: IBCSO VERSION 1.0, Geophys. Res. Lett., 40, 3111–3117, https://doi.org/10.1002/grl.50413, 2013.

Berkman, P. A.: The population biology of the Atarctic scallop, Adamussium colbecki (Smith 1902) at New Harbor, Ross Sea, in: Antarctic Ecosystems, edited by: Kerry, K.R. and Hempel, G., Springer, Berlin, Heidelberg, Germany, 281–288, https://doi.org/10.1007/978-3-642-84074-6_32, 1990.

Black, H., and Andrus, C. F. T.: Taphonomy and diagenesis on the deep-sea hydrocoral Stylaster erubescens fossils from the Charleston Bump, Univ Alabama McNair J, 12, 19-40, 2012.

Braga-Henriques A., Carreiro-Silva M., Porteiro F.M., de Matos V., Sampaio I., Ocaña O., and Avila S.P.: The association between a deep-sea gastropod Pedicularia sicula and its coral host Errina dabneyi in the Azores. ICES J. Mar. Sci. 68: 399–407, http://doi.org/10.1093/icesjms/fsq066, 2010.

Burke, A. and Robinson, L. F.: The Southern Ocean's Role in Carbon Exchange During the Last Deglaciation, Science, 335, 557–561, https://doi.org/10.1126/science.1208163, 2012.

Cairns, S. D.: A generic revision of the Stylasterina (Coelenterata: Hydrozoa). Part 1, Description of the genera, B. Mar. Sci., 33, 427-508, 1983a.

Cairns, S. D.: Antarctic and Subantarctic Stylasterina (Coelenterata: Hydrozoa), in: Biology of the Antarctic Seas XIII, vol. 38, edited by: Kornicker, S., American Geophysical Union, Washington, D. C., USA, 61–164, 1983b.

Cairns, S. D.: A generic revision of the Stylasteridae (Coelenterata: Hydrozoa). (Coelenterata: Hydrozoa). Part 3, Keys to the genera, B. Mar. Sci., 49, 538-545, 1991.

Cairns, S. D.: Worldwide distribution of the Stylasteridae (Cnidaria: Hydrozoa), Sci. Mar., 56, 125–130, 1992.

Cairns, S. D. and Macintyre, I. G.: Phylogenetic Implications of Calcium Carbonate Mineralogy in the Stylasteridae (Cnidaria: Hydrozoa), PALAIOS, 7, 96-107, https://doi.org/10.2307/3514799, 1992.

Chen, S., Gagnon, A. C., and Adkins, J. F.: Carbonic anhydrase, coral calcification and a new model of stable isotope vital effects, Geochim. Cosmochim. Ac., 236, 179–197, https://doi.org/10.1016/j.gca.2018.02.032, 2018.

Chen, T., Robinson, L. F., Burke, A., Claxton, L., Hain, M. P., Li, T., Rae, J. W. B., Stewart, J., Knowles, T. D. J., Fornari, D. J., and Harpp, K. S.: Persistently well-ventilated intermediate-depth ocean through the last deglaciation, Nat. Geosci., https://doi.org/10.1038/s41561-020-0638-6, 2020.

Chong, A. K., and Stratford, P.: Underwater digital stereo-observation technique for red hydrocoral study. Photogramm. Eng. Rem. S., 68(7), 745–752, 2002.

Druffel, E. R. M.: Geochemistry of corals: Proxies of past ocean chemistry, ocean circulation, and climate, P. Natl. Acad. Sci., 94, 8354–8361, https://doi.org/10.1073/pnas.94.16.8354, 1997.

Druffel, E. R. M., King, L. L., Belastock, R. A., and Buesseler, K. O.: Growth rate of a deep-sea coral using 210Pb and other isotopes, Geochim. Cosmochim. Ac., 54, 1493–1499, https://doi.org/10.1016/0016-7037(90)90174-J, 1990.

Emiliani, C.: Pleistocene temperatures, J. Geol., 63, 538–578, https://doi.org/10.1086/626295, 1955.

Emiliani, C., Hudson, J. H., Shinn, E. A., and George, R. Y.: Oxygen and carbon isotopic growth record in a reef coral from the Florida Keys and a deep-sea coral from Blake Plateau, Science, 202, 627–629, https://doi.org/10.1126/science.202.4368.627, 1978.

Epstein, S., Buchsbaum, R., Lowenstam, H., and Urey, H. C.: Carbonate-water isotopic temperature scale, Geol. Soc. Am. Bull., 62, 417–426, https://doi.org/10.1130/0016-7606(1951)62[417:CITS]2.0.CO;2, 1951.

Epstein, S., Buchsbaum, R., Lowenstam, H., and Urey, H. C.: Revised carbonate-water isotopic temperature scale, Bull. Geol. Soc. Am., 64, 1315–1326, https://doi.org/10.1130/0016-7606(1953)64[1315:RCITS]2.0.CO;2, 1953.

Fallon, S. J., Thresher, R. E., and Adkins, J.: Age and growth of the cold-water scleractinian Solenosmilia variabilis and its reef on SW Pacific seamounts, Coral Reefs, 33, 31–38, https://doi.org/10.1007/s00338-013-1097-y, 2014.

Gerrish, L., Fretwell, P., & Cooper, P., High resolution vector polylines of the Antarctic coastline (7.5), UK Polar Data Centre, Natural Environment Research Council, UK Research & Innovation [Basemap] https://doi.org/10.5285/bc71347d-298a-4df3-88b0-cb9a908db166, 2022.

Gladfelter, E. H.: Skeletal development in Acropora cervicornis: I. Patterns of calcium carbonate accretion in the axial corallite, Coral Reefs, 1, 45–51, https://doi.org/10.1007/BF00286539, 1982.

Gladfelter, E. H.: Skeletal Development in Acropora cervicornis: II. Diel patterns of calcium carbonate accretion, Coral Reefs, 2, 91–100, https://doi.org/10.1007/BF02395279, 1983.

Gladfelter, E. H.: Skeletal Development in Acropora cervicornis: III. A comparison of monthly rates of linear extension and calcium carbonate accretion measured over a year, Coral Reefs, 3, 51–57, https://doi.org/10.1007/BF00306140, 1984.

Gordon, A.: Calibrated Hydrographic Data acquired with a CTD in the Ross Sea during the Nathaniel B. Palmer expedition NBP0302 (2003), Interdisciplinary Earth Data Alliance [CTD/Rosette], http://doi.org/10.1594/IEDA/317291, 2016.

Gordon, A. L., Orsi, A. H., Muench, R., Huber, B. A., Zambianchi, E., and Visbeck, M.: Western Ross Sea continental slope gravity currents, Deep-Sea Res. Pt. II, 56, 796–817, https://doi.org/10.1016/j.dsr2.2008.10.037, 2009.

Griffin, S. and Druffel, E. R. M.: Sources of Carbon to Deep-Sea Corals, Radiocarbon, 31, 533–543, https://doi.org/10.1017/S0033822200012121, 1989.

Grossman, E. L. and Ku, T.-L.: Oxygen and carbon isotope fractionation in biogenic aragonite: temperature effects, Chem. Geol. (Isotope Geoscience Section), 59, 59-74, https://doi.org/10.1016/0168-9622(86)90057-6, 1986.

Heikoop, J. M., Dunn, J. J., Risk, M. J., Schwarcz, H. P., McConnaughey, T. A., and Sandeman, I. M.: Separation of kinetic and metabolic isotope effects in carbon-13 records preserved in reef coral skeletons, Geochim. Cosmochim. Ac., 64, 975–987, https://doi.org/10.1016/S0016-7037(99)00363-4, 2000.

Hill, T. M., Spero, H. J., Guilderson, T., LaVigne, M., Clague, D., Macalello, S., and Jang, N.: Temperature and vital effect controls on bamboo coral (*Isididae*) isotope geochemistry: A test of the “lines method”, Geochem. Geophy. Geosy., 12, 14, https://doi.org/10.1029/2010GC003443, 2011.

Houlbrèque, F., Meibom, A., Cuif, J.-P., Stolarski, J., Marrocchi, Y., Ferrier-Pagès, C., Domart-Coulon, I., and Dunbar, R. B.: Strontium-86 labeling experiments show spatially heterogeneous skeletal formation in the scleractinian coral *Porites porites*, Geophys. Res. Lett., 36, L04604, https://doi.org/10.1029/2008GL036782, 2009.

Jacobs, S.: Calibrated Hydrographic Data from the Ross Sea acquired with a CTD during the Nathaniel B. Palmer expedition NBP0408 (2004), Interdisciplinary Earth Data Alliance [CTD/Rosette], http://doi.org/10.1594/IEDA/307443, 2015.

Jacobs, S. S., Fairbanks, R. G., and Horibe, Y. G.: Origin and evolution of water masses near the Antarctic continental margin: Evidence from H218O/H216O ratios in seawater, in: Antarctic Research Series, vol. 43, edited by: Jacobs, S., American Geophysical Union, Washington, D. C., 59–85, https://doi.org/10.1029/AR043p0059, 1985.

Jacobs, S. S., Amos, A. F., and Bruchhausen, P. M.: Ross Sea oceanography and Antarctic Bottom Water formation, Deep-Sea Res. and Oceanographic Abstracts, 17, 935–962, https://doi.org/10.1016/0011-7471(70)90046-X, 1970.

King, T. M., Rosenheim, B. E., Post, A. L., Gabris, T., Burt, T., and Domack, E. W.: Large-scale intrusion of circumpolar deep water on Antarctic margin recorded by stylasterid corals, Paleoceanography and Paleoclimatology, 33(11), 1306–1321, http://doi.org/10.1029/2018PA003439, 2018.

Kurtz, D. D. and Bromwich, D. H.: A recurring, atmospherically forced polynya in Terra Nova Bay, in: Oceanology of the Antarctic Continental Shelf, vol. 43, edited by: Jacobs, S., American Geophysical Union, Washington, D. C., USA, 177–201, 1985.

Matsuoka, K., Skoglund, A., Roth, G., de Pomereu, J., Griffiths, H., Headland, R., Herried, B., Katsumata, K., Le Brocq, A., Licht, K., Morgan, F., Neff, P. D., Ritz, C., Scheinert, M., Tamura, T., Van de Putte, A., van den Broeke, M., von Deschwanden, A., Deschamps-Berger, C., Van Liefferinge, B., Tronstad, S., and Melvær, Y.: Quantarctica, an integrated mapping environment for Antarctica, the Southern Ocean, and sub-Antarctic islands, Environ. Modell. Softw., 140, 105015, https://doi.org/10.1016/j.envsoft.2021.105015, 2021.

McConnaughey, T.: 13C and 18O isotopic disequilibrium in biological carbonates: I. Patterns, Geochim. Cosmochim. Ac., 53, 151-162, https://doi.org/10.1016/0016-7037(89)90282-2, 1989a.

McConnaughey, T.: 13C and 18O isotopic disequilibrium in biological carbonates II. In vitro simulation of kinetic isotope effects, Geochim. Cosmochim. Ac., 53, 163–171, https://doi.org/10.1016/0016-7037(89)90283-4, 1989b.

McCrea, J. M.: On the Isotopic Chemistry of Carbonates and a Paleotemperature Scale, J. Chem. Phys., 18, 849–857, https://doi.org/10.1063/1.1747785, 1950.

Mikkelsen, N., Erlenkeuser, H., Killingley, J. S., and Berger, W. H.: Norwegian corals: radiocarbon and stable isotopes in Lophelia pertusa, Boreas, 11, 163–171, https://doi.org/10.1111/j.1502-3885.1982.tb00534.x, 2008.

Miller, K. J., Mundy, C. N., and Chadderton, W. L.: Ecological and genetic evidence of the vulnerability of shallow-water populations of the stylasterid hydrocoral *Errina novaezelandiae* in New Zealand's fiords. Aquat. Conserv., 14(1), 75–94, https://doi.org/10.1002/aqc.597, 2004.

Mouginot, J., B. Scheuchl, and E. Rignot. 2017. MEaSUREs Antarctic Boundaries for IPY 2007-2009 from Satellite Radar, Version 2 [Coastline and grounding line], Boulder, Colorado USA. NASA National Snow and Ice Data Center Distributed Active Archive Center, http://dx.doi.org/10.5067/AXE4121732AD, https://nsidc.org/data/nsidc-0709/versions/2, 2022.

O'Neil, J. R., Clayton, R. N., and Mayeda, T. K.: Oxygen Isotope Fractionation in Divalent Metal Carbonates, J. Chem. Phys., 51, 5547–5558, https://doi.org/10.1063/1.1671982, 1969.

Philipp, E., Brey, T., Pörtner, H.-O., and Abele, D.: Chronological and physiological ageing in a polar and a temperate mud clam, Mech. Ageing Dev., 126, 598–609, https://doi.org/10.1016/j.mad.2004.12.003, 2005.

Pica, D., Cairns, S. D., Puce, S., and Newman, W. A.: Southern hemisphere deep-water stylasterid corals including a new species, Errina labrosa sp. n. (Cnidaria, Hydrozoa, Stylasteridae), with notes on some symbiotic scalpellids (Cirripedia, Thoracica, Scalpellidae), ZooKeys, (472), 1, http://doi.org/10.3897/zookeys.472.8547, 2015.

Picco, P., Bergamasco, A., Demicheli, L., Manzella, G., Meloni, R., and Paschini, E.: Large-scale circulation features in the Central and Western Ross Sea (Antarctica), in: Ross Sea Ecology, Springer, Berlin, Heidelberg, Germany, 95–105, 2000.

Puce, S., Tazioli, S., and Bavestrello, G.: First evidence of a specific association between a stylasterid coral (Cnidaria: Hydrozoa: Stylasteridae) and a boring cyanobacterium, Coral Reefs, 28, 177-177, https://doi.org/10.1007/s00338-008-0411-6, 2009.

Puce, S., Pica, D., Mancini, L., Brun, F., Peverelli, A., and Bavestrello, G.: Three-dimensional analysis of the canal network of an Indonesian Stylaster (Cnidaria, Hydrozoa, Stylasteridae) by means of X-ray computed microtomography. Zoomorphology 130, 85–95, https://doi.org/10.1007/s00435-011-0120-5, 2011.

Ralph, R. and Maxwell, J. G. H.: Growth of two Antarctic lamellibranchs: Adamussium colbecki and Laternula elliptica, Mar. Biol., 42, 171–175, https://doi.org/10.1007/BF00391569, 1977.

Risk, M. J., Heikoop, J. M., Snow, M. G., and Beukens, R.: Lifespans and growth patterns of two deep-sea corals: Primnoa resedaeformis and Desmophyllum cristagalli, Hydrobiologia, 471, 125–131, https://doi.org/10.1023/A:1016557405185, 2002.

Robinson, L. F. and van de Flierdt, T.: Southern Ocean evidence for reduced export of North Atlantic Deep Water during Heinrich event 1, Geology, 37, 195–198, https://doi.org/10.1130/G25363A.1, 2009.

Robinson, L. F., Adkins, J., Keigwin, L. D., Southon, J., Fernandez, D. P., Wang, S.-L., and Scheirer, D. S.: Radiocarbon variability in the Western North Atlantic during the Last Deglaciation, Science, 310, 1469–1473, https://doi.org/10.1126/science.1114832, 2005.

Robinson, L. F., Adkins, J. F., Frank, N., Gagnon, A. C., Prouty, N. G., Brendan Roark, E., and de Flierdt, T. van: The geochemistry of deep-sea coral skeletons: A review of vital effects and applications for palaeoceanography, Deep-Sea Res. Pt. II: Topical Studies in Oceanography, 99, 184–198, https://doi.org/10.1016/j.dsr2.2013.06.005, 2014.

Romanek, C. S., Grossman, E. L., and Morse, J. W.: Carbon isotopic fractionation in synthetic aragonite and calcite: Effects of temperature and precipitation rate, Geochim. Cosmochim. Ac., 56, 419–430, https://doi.org/10.1016/0016-7037(92)90142-6, 1992.

Román-González, A., Scourse, J. D., Butler, P. G., Reynolds, D. J., Richardson, C. A., Peck, L. S., Brey, T., and Hall, I. R.: Analysis of ontogenetic growth trends in two marine Antarctic bivalves Yoldia eightsi and Laternula elliptica: Implications for sclerochronology, Palaeogeogr. Palaeoecol., 465, 300–306, https://doi.org/10.1016/j.palaeo.2016.05.004, 2017.

Samperiz, A., Robinson, L. F., Stewart, J. A., Strawson, I., Leng, M. J., Rosenheim, B. E., Ciscato, E. R., Hendry, K. R., and Santodomingo, N.: Stylasterid corals: A new paleotemperature archive, Earth Planet. Sc. Lett., 545, 116407, https://doi.org/10.1016/j.epsl.2020.116407, 2020.

Sandrini, S., Ait-Ameur, N., Rivaro, P., Massolo, S., Touratier, F., Tositti, L., and Goyet, C.: Anthropogenic carbon distribution in the Ross Sea, Antarctica, Antarct. Sci., 19, 395–407, https://doi.org/10.1017/S0954102007000405, 2007.

Shackleton, N.: Oxygen isotope analyses and Pleistocene temperatures re-assessed, Nature, 215, 15–17, https://doi.org/10.1038/215015a0, 1967.

Smith, J. E., Schwarcz, H. P., Risk, M. J., McConnaughey, T. A., and Keller, N.: Paleotemperatures from deep-sea corals: overcoming 'vital effects,' PALAIOS, 15, 25–32, 2000.

Smith, J. E., Schwarcz, H. P., and Risk, M. J.: Patterns of isotopic disequilibria in azooxanthellate coral skeletons, Hydrobiologia, 471, 111–115, https://doi.org/10.1023/A:1016553304276, 2002.

Stewart, J.A., Robinson, L.F., Day, R.D., Strawson, I., Burke, A., Rae, J.W., Spooner, P.T., Samperiz, A., Etnoyer, P.J., Williams, B., Paytan, A., Leng, M.J., Häussermann, V., Wickes, L.N., Bratt, R., and Pryer, H.: Refining trace metal temperature proxies in cold-water scleractinian and stylasterid corals, Earth Planet. Sc. Lett., 545, p.116412, http://doi.org/10.1016/j.epsl.2020.116412, 2020.

Stratford, P., Stewart, B. G., and Chong, A.: In situ growth rate measurements on the red hydrocoral, *Errina novaezelandiae*, in Doubtful Sound, New Zealand fjords: Researching, managing, and conserving a unique ecosystem, New Zeal. J. Mar. Fresh., 35(4), 653–661. https://doi.org/10.1080/00288330.2001.9517032, 2001.

Swart, P. K.: Carbon and oxygen isotope fractionation in scleractinian corals: a review, Earth-Sci. Rev., 19, 51–80, https://doi.org/10.1016/0012-8252(83)90076-4, 1983.

Thresher, R., Tilbrook, B., Fallon, S., Wilson, N., and Adkins, J.: Effects of chronic low carbonate saturation levels on the distribution, growth and skeletal chemistry of deep-sea corals and other seamount megabenthos, Mar. Ecol. Prog. Ser., 442, 87–99, https://doi.org/10.3354/meps09400, 2011.

Urey, H. C.: The thermodynamic properties of isotopic substances, J. Chem. Soc. (Resumed), 562–581, https://doi.org/10.1039/jr9470000562, 1947.

Urushihara, Y., Hasegawa, H., and Iwasaki, N.: X-ray micro-CT observation of the apical skeleton of Japanese white coral Corallium konojoi, J. Exp. Mar. Biol. Ecol., 475, 124–128, https://doi.org/10.1016/j.jembe.2015.11.016, 2016.

Visbeck, M.: Calibrated Hydrographic Data from the Ross Sea acquired with a CTD during the Nathaniel B. Palmer expedition NBP0402 (2004), Interdisciplinary Earth Data Alliance [CTD/Rosette], http://doi.org/10.1594/IEDA/307431, 2015.

Weber, J. N.: Deep-sea ahermatypic scleractinian corals: isotopic composition of the skeleton, Deep-Sea Res. and Oceanographic Abstracts, 20, 901–909, https://doi.org/10.1016/0011-7471(73)90108-3, 1973.

Weber, J. N. and Woodhead, P. M. J.: Carbon and oxygen isotope fractionation in the skeletal carbonate of reef-building corals, Chem. Geol., 6, 93–117, https://doi.org/10.1016/0009-2541(70)90009-4, 1970.

Wisshak, M., López Correa, M., Zibrowius, H., Jakobsen, J., and Freiwald, A.: Skeletal reorganisation affects geochemical signals, exemplified in the stylasterid hydrocoral Errina dabneyi (Azores Archipelago), Mar. Ecol. Prog. Ser., 397, 197–208, https://doi.org/10.3354/meps08165, 2009.

Wisshak, M., Form, A., Jakobsen, J., and Freiwald, A.: Temperate carbonate cycling and water mass properties from intertidal to bathyal depths (Azores), Biogeosciences, 7, 2379–2396, https://doi.org/10.5194/bg-7-2379-2010, 2010.

WOCE Hydrographic Programme, WHP: Hydrochemistry measured on water bottle samples during Akademik Ioffe cruise 90KDIOFFE6_1 on section S04P, PANGAEA [CTD/Rosette], https://doi.org/10.1594/PANGAEA.837058, 2002.